

# A one-dimensional three-state run-and-tumble model with a ‘cell cycle’

Davide Breoni<sup>a,1</sup>, Fabian Jan Schwarzendahl<sup>1</sup>, Ralf Blossey<sup>2</sup>, Hartmut Löwen<sup>1</sup>

<sup>1</sup>Institut für Theoretische Physik II: Weiche Materie, Heinrich-Heine-Universität Düsseldorf, Universitätsstraße 1, 40225 Düsseldorf, Germany

<sup>2</sup>University of Lille, Unité de Glycobiologie Structurale et Fonctionnelle (UGSF), CNRS UMR8576, 59000 Lille, France

Received: date / Accepted: date

**Abstract** We study a one-dimensional three-state run-and-tumble model motivated by the bacterium *Caulobacter crescentus* which displays a cell cycle between a non-proliferation mobile phase and a proliferating sedentary phase. Our model implements kinetic transitions between the two mobile and one sedentary states described in terms of their probability densities, where mobility is allowed with different activities in forward and backward direction. We start by analyzing the stationary states of the system and compute the mean squared displacement, which shows a surprising super-ballistic scaling at early times. Including interactions between the three states, we explore the stability of the system and then employ numerical methods to study structure formation in the fully nonlinear system. We find traveling waves of bacteria, whose occurrence is quantified in a non-equilibrium state diagram.

## 1 Introduction

The run-and-tumble (RT) model describes a class of active systems which is originally motivated by the motion of bacteria propelled by their flagellae. The flagella motor generates a torque which translates into forward or back motion of the bacteria. This motion only persists for a finite time, the ‘run’-time, after which the bacterium stalls, the ‘tumble’-period, before continuing its motion typically in a different direction [1–14].

RT models in one dimension are a special case within this model class. Here, the bacterium can only switch between left- and right motion in a stochastic manner. One-dimensional RT-models have proven to be an extremely rich reservoir for analytic calculations - in some sense, they are like the analogue of Ising models in active systems [15–22].

Carrying this analogy further, several works have appeared in the very recent past in which the number of ‘states’ in which the bacterium can find itself go beyond the two left- and right-moving states. Models with three and more states have been discussed - in our Ising-model analogy, this would amount to looking at active analogues of ‘Potts’-type models [23–25].

The present paper inserts itself in this line of research by considering a three-state RT model with the states: left-moving, right-moving and sedentary. Our model is motivated by the behavior of the bacterium *Caulobacter crescentus* (*CC*) which is a model organism in microbiology since it has a complex lifestyle [26, 27] *CC* has a cell-cycle: in order to undergo cell division, the bacterium has to switch from its mobile swarmer state to a spatially localized stalked state. Only from the latter state the proliferation of new cells is possible. Our model is not limited to *CC* or bacteria. E.g., the green algae *Chlamydomonas reinhardtii* has a similar cell cycle [28] with sedentary and swimming states and also performs a run-and-tumble motion [2].

The paper is organized as follows. In section 2, we develop our RT-model inspired by *CC* in detail and discuss the relevant parameter regimes. In section 3, we first focus on the free cell case of the model which enables us to make analytical predictions. We derive the conditions for stability of the system when spatial dependencies are neglected. Adding the spatial dependence we study the mean displacement and mean squared displacement for a single cell in the process of duplicating, both showing a surprising  $t^3$  regime for short times. Then, in section 4, we allow the cells to interact via both mechanisms of attraction and repulsion.

<sup>a</sup>e-mail: breoni@hhu.de

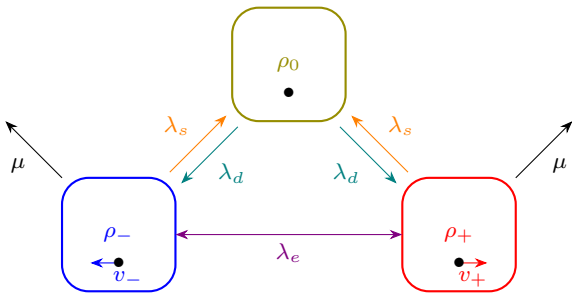


**Fig. 1** Graphical representation of the transition rates among different species. These transitions are motivated by the cell cycle of *Caulobacter crescentus*, that either moves actively or settles down to reproduce. Our model contains three different species: the cells moving to the right  $\rho_+$ , those moving to the left  $\rho_-$  and the settled ones  $\rho_0$ . The moving cells can either settle via the rate  $\lambda_s$ , move in the opposite direction with  $\lambda_e$  or die with  $\mu$ . Settled cells duplicate via  $\lambda_d$ , and generate both a left- and a right-moving cell.

From this antagonistic effect, we numerically observed structure formation: we find traveling waves of bacteria and quantify their occurrence in a non-equilibrium state diagram. We end the paper with our conclusions and an outlook in section 5.

## 2 Model

Inspired by the reproductive behavior of *Caulobacter crescentus* we consider a 1D toy-model representing bacteria that can actively move rightward, leftward or settle down, and that when settled double in number. This ‘cell cycle’ of our three-state RT model motivated by *CC* is summarized in Figure 1. We allow for three populations with probability densities  $\rho_+(x, t)$ ,  $\rho_-(x, t)$  and  $\rho_0(x, t)$ , functions of space  $x$  and time  $t$ , respectively corresponding to right and left movers, and to the sedentary population. The ‘cell cycle’ step is given by the rate of settling down,  $\lambda_s$ , which can occur from either moving state, and the cell doubling with rate  $\lambda_d$  with which a sedentary bacterium gives rise to a pair of right- and left-moving cells. Exchange of direction, i.e. the RT step, is denoted by  $\lambda_e$ . Finally,  $\mu$  is the dying rate, which we consider for motile cells only. In a proliferating system, this rate prevents exponential growth. This idealized *CC*-‘cell cycle’ is then implemented in terms of Fokker-Planck equations for the probability densities.

As the bacteria are micron-sized swimmers, we assume a low Reynolds number and overdamped dynamics. To describe this behavior mathematically we introduce a system of Fokker-Planck equations for the probability densities of three species with probability

|                                 |             |                          |
|---------------------------------|-------------|--------------------------|
| run-and-tumbling rate; $s^{-1}$ | $\lambda_e$ | $10^{-3}$                |
| settling rate; $s^{-1}$         | $\lambda_s$ | $10^{-5}$                |
| doubling rate; $s^{-1}$         | $\lambda_d$ | $10^{-4}$                |
| decay rate; $s^{-1}$            | $\mu$       | $10^{-6}$                |
| running speed right; $m/s$      | $v_+$       | $4 \cdot 10^{-5}$        |
| running speed left; $m/s$       | $v_-$       | $4 \cdot 10^{-5} - 10\%$ |
| diffusion coefficient; $m^2/s$  | $D$         | $2 \cdot 10^{-9}$        |

**Table 1** Values of the parameters for *Caulobacter crescentus* taken from [29–32].

densities  $\rho_+(x, t)$ ,  $\rho_-(x, t)$  and  $\rho_0(x, t)$ :

$$\begin{aligned}
 \partial_t \rho_+ &= -v_+ \partial_x \rho_+ + \partial_x (\partial_x U \rho_+) + D \partial_x^2 \rho_+ \\
 &\quad - (\lambda_s + \lambda_e + \mu) \rho_+ + \lambda_e \rho_- + \lambda_d \rho_0 \\
 \partial_t \rho_0 &= \partial_x (\partial_x V \rho_0) - \lambda_d \rho_0 + \lambda_s (\rho_+ + \rho_-) \\
 \partial_t \rho_- &= v_- \partial_x \rho_- + \partial_x (\partial_x U \rho_-) + D \partial_x^2 \rho_- \\
 &\quad - (\lambda_s + \lambda_e + \mu) \rho_- + \lambda_e \rho_+ + \lambda_d \rho_0.
 \end{aligned} \tag{1}$$

Here,  $D$  is the diffusion coefficient for the actively moving cells,  $U[\rho_0]$  is the potential acting on  $\rho_{\pm}$  and  $V[\rho_0]$  is the one acting on  $\rho_0$ , both being functionals of  $\rho_0$ . All coefficients are positive.

Table 1 gives an idea of the experimentally measured values for *CC* which have been extracted from recent papers on its swimming behaviour [29–32]. It is noteworthy to comment on the activities  $v_+$ ,  $v_-$ . While the torque generated by the flagellar motor differs significantly during forward and backward motion, the resulting velocities are not dramatically different (and, in fact, experimentally hard to measure) [32]. We take the difference as up to 10 %.

## 3 Free cells

We start by setting  $U = V = 0$ , and hence consider free cells. In this case the system of differential equations is linear and can be solved analytically via matrix calculations. In order to perform these matrix operations we summarize the densities in a 3-component vector  $\rho = (\rho_+, \rho_0, \rho_-)$ .

### 3.1 Population dynamics

First, we consider the number of cells in the system by computing  $\bar{\rho}(t) \equiv \int_{-\infty}^{\infty} \rho(x, t) dx$ . When we integrate Eqs. (1) over  $x$ , the space derivatives reduce to boundary values. Assuming that  $\rho(\pm\infty, t) = \partial_x \rho(\pm\infty, t) = 0$ , this lets us drop the spatial terms, so that we can focus on the population exchange and growth dynamics. We

can write the resulting equation system in matrix form:

$$\dot{\bar{\rho}}(t) = \mathcal{M}\bar{\rho}(t), \quad (2)$$

where

$$\mathcal{M} = \begin{pmatrix} -(\lambda_s + \lambda_e + \mu) & \lambda_d & \lambda_e \\ \lambda_s & -\lambda_d & \lambda_s \\ \lambda_e & \lambda_d & -(\lambda_s + \lambda_e + \mu) \end{pmatrix}. \quad (3)$$

The solution for this system of differential equations is

$$\bar{\rho}(t) = e^{\mathcal{M}t}\bar{\rho}(0) = \mathcal{P}e^{\mathcal{E}t}\mathcal{P}^{-1}\bar{\rho}(0). \quad (4)$$

$\mathcal{P}$  is the eigenvector matrix of  $\mathcal{M}$  and  $\mathcal{E}$  is the diagonal matrix containing the eigenvalues of  $\mathcal{M}$ , that are

$$\begin{aligned} \mathcal{E}_1 &= -(\mu + 2\lambda_e + \lambda_s) \\ \mathcal{E}_2 &= -(\mu + \lambda_d + \lambda_s + \Lambda)/2 \\ \mathcal{E}_3 &= -(\mu + \lambda_d + \lambda_s - \Lambda)/2, \end{aligned} \quad (5)$$

where  $\Lambda = \sqrt{(\mu + \lambda_d + \lambda_s)^2 + 4\lambda_d(\lambda_d - \mu)}$ . We notice that the first two eigenvalues are always negative and therefore stable, while the sign of the third one depends on  $\lambda_s - \mu$ , which can become unstable. This instability facilitates an exponential growth of the colony. In fact, for small values of  $\lambda_s - \mu$  the unstable eigenvalue becomes

$$\begin{aligned} \mathcal{E}_3 &= -\frac{\mu + \lambda_d + \lambda_s}{2} \left( 1 - \sqrt{1 + \frac{4\lambda_d(\lambda_s - \mu)}{(\mu + \lambda_d + \lambda_s)^2}} \right) \\ &\simeq \frac{\lambda_d(\lambda_s - \mu)}{\mu + \lambda_d + \lambda_s}. \end{aligned} \quad (6)$$

This means that the exponential growth or collapse of the system is decided by the difference of  $\lambda_s$  and  $\mu$ , or in different terms, that the separating line between the two behaviors is  $\lambda_s = \mu$ . It is also worth pointing out that in the case of instant doubling, that is the limit of  $\lambda_d \rightarrow \infty$ ,  $\mathcal{E}_3$  simply reduces to  $\lambda_s - \mu$ , as can be seen in Figure 2. Physically this is expected, as in this model cells can double only when settled and can die only when moving, meaning that the growth or decay of the system size depends exclusively on whether a moving cell is faster in settling or dying. In real life both the settling and doubling rates are much larger than the dying rate, as can be seen in Table 1, but we can assume that the system has already reached maximum capacity and that the available resources do not allow for more growth. In this case, i.e.  $\mu = \lambda_s$ , the number of cells is stable for long times and it is possible to calculate the

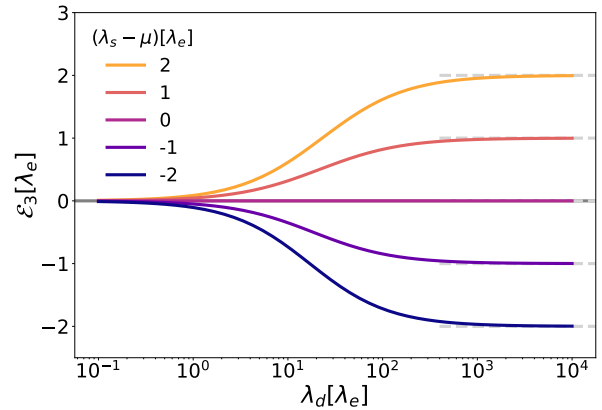


**Fig. 2** Unstable eigenvalue  $\mathcal{E}_3$  (solid lines) as a function of doubling rate  $\lambda_d$  for different values of  $\lambda_s$  (color code) and  $\mu = 10\lambda_e$ . The sign of  $\mathcal{E}_3$  is the same of  $\lambda_s - \mu$ , and its value also stabilizes at  $\lambda_s - \mu$  for very large values of  $\lambda_d$  (dashed lines).

stationary value of  $\bar{\rho}(t \rightarrow \infty)$  as a function of the initial conditions  $\bar{\rho}(0)$ :

$$\begin{aligned} \bar{\rho}_+(t \rightarrow \infty) &= \frac{\lambda_d}{2(2\mu + \lambda_d)} R(0) \\ \bar{\rho}_0(t \rightarrow \infty) &= \frac{\mu}{2\mu + \lambda_d} R(0) \\ \bar{\rho}_-(t \rightarrow \infty) &= \frac{\lambda_d}{2(2\mu + \lambda_d)} R(0), \end{aligned} \quad (7)$$

where  $R(0) = 2\bar{\rho}_0(0) + \bar{\rho}_-(0) + \bar{\rho}_+(0)$ . Since the exchange rate between right  $\bar{\rho}_+$  and left  $\bar{\rho}_-$  moving cells is symmetric, the amounts of left and right moving cells are the same in the stationary state ( $\bar{\rho}_+ = \bar{\rho}_-$ , see also Figure 3). Furthermore, if  $\lambda_d = 2\mu = 2\lambda_s$  all the three populations equilibrate to the same value, independently of the initial conditions.

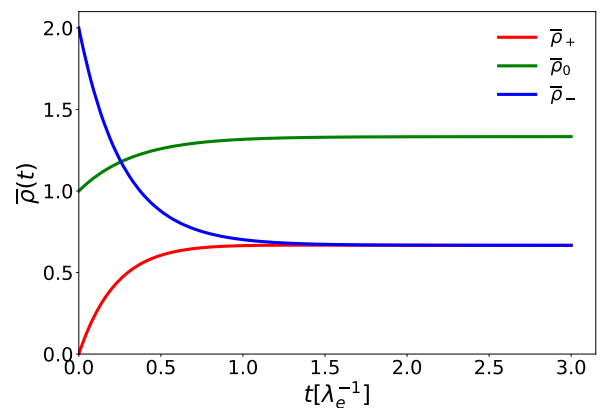


**Fig. 3** Amount of right-  $\bar{\rho}_+$ , left-moving  $\bar{\rho}_-$  and sedentary  $\bar{\rho}_0$  cells as functions of time. All rates are set to be equal to  $\lambda_e$  and the initial conditions are  $\bar{\rho}(0) = (0, 1, 2)$ .

### 3.2 Density dynamics

We study now the evolution of the spatial quantities of the system, such as the mean displacement  $MD = \langle x - x_0 \rangle$ , the mean squared displacement  $MSD = \langle (x - x_0)^2 \rangle$  and all the higher order moments, where  $x_0$  is the average position of the system at  $t = 0$ . Here, the average  $\langle (\cdot) \rangle$  is defined as  $\int_{-\infty}^{\infty} (\rho_+ + \rho_0 + \rho_-)(\cdot) dx$ . In order to compute averages, we first solve the system by using a Fourier transform  $FT$ :

$$\dot{\tilde{\rho}}(k, t) = \tilde{\mathcal{M}}(k) \tilde{\rho}(k, t), \quad (8)$$

where  $\tilde{\rho}(k, t) = FT(\rho(x, t))$  is the Fourier transform of  $\rho(x, t)$ ,  $k$  is the wave number conjugate to  $x$  and

$$\tilde{\mathcal{M}}(k) = \mathcal{M} - \begin{pmatrix} k^2 D + ikv_+ & 0 & 0 \\ 0 & 0 & 0 \\ 0 & 0 & k^2 D - ikv_- \end{pmatrix}. \quad (9)$$

Similarly to the constant density case, the solution in Fourier space will be given by

$$\tilde{\rho}(k, t) = e^{\tilde{\mathcal{M}}(k)t} \tilde{\rho}(k, 0). \quad (10)$$

One can use the solution of this equation to extract the intermediate scattering function

$$\mathcal{F}(k, t) \equiv \frac{\tilde{\rho}(k, t) \cdot \tilde{\rho}(-k, 0)}{N(0)}, \quad (11)$$

where  $N(t) \equiv \bar{\rho}_0(t) + \bar{\rho}_+(t) + \bar{\rho}_-(t)$  is the total number of cells. The intermediate scattering function can be related to the various moments of the density [33] by:

$$\langle (x(t) - x_0)^n \rangle = \frac{i^n}{N(t)} \left. \frac{\partial^n}{\partial k^n} \mathcal{F}(k, t) \right|_{k=0}, \quad (12)$$

which is valid in one dimension (see Appendix). For simplicity, we will consider as initial conditions  $\rho(x, 0) = (0, \delta(x), 0)$ . These are physically relevant, as they describe a cell initially settled in  $x = 0$  in the process of reproducing. When the system is asymmetric, i.e.  $v_+ \neq v_-$ , the MD is non-zero and we can see two different regimes: for short times it grows as  $t^3$ , while for long times it is proportional to  $t$ , as shown in Figure 4(a). The short time expansion of the MD in fact yields

$$\begin{aligned} \langle x(t) - x_0 \rangle &= \frac{1}{6} \lambda_s \lambda_d (v_+ - v_-) t^3 \\ &\quad - \frac{1}{12} \lambda_s \lambda_d (v_+ - v_-) (\mu + 3\lambda_d + \lambda_s) t^4 \\ &\quad + \mathcal{O}(t^5), \end{aligned} \quad (13)$$

showing that both the transition rates and the activity have a role in determining this initial scaling regime.

This can be seen as a composition of the doubling mechanism and the system acceleration given by cells suddenly starting to move. We can further define the typical crossover time  $t_c^{(1)}$  as the ratio between absolute values of the coefficients of the  $t^3$  and  $t^4$  scalings, as this is the time at which the  $t^3$  order contribution becomes smaller than the following ones. This is a good estimate of the average time at which the dynamics is not dominated by the initial doubling anymore:

$$t_c^{(1)} = \frac{2}{\mu + 3\lambda_d + \lambda_s}. \quad (14)$$

For what concerns the MSD, in Figure 4(b) we still see a  $t^3$  regime for short times, while the long time behavior depends on the difference between  $v_-$  and  $v_+$ . In case they are the same, we will only see a diffusive long time regime, otherwise this diffusive regime transitions into a ballistic one. The diffusive and ballistic regimes become more distinguishable when  $v_+$  and  $v_-$  have similar, yet different, values. We further calculate the short time expansion of the MSD. Here, we assume that active speeds are the same  $v_{\pm} = v$ , since the swimming speeds of  $CC$  differ by only 10% (Table 1):

$$\begin{aligned} \langle (x(t) - x_0)^2 \rangle &\simeq \frac{2}{3} D \lambda_s \lambda_d t^3 \\ &\quad - \frac{1}{6} \lambda_s \lambda_d (2D(\mu + 3\lambda_d + \lambda_s) - v^2) t^4 \\ &\quad + \mathcal{O}(t^5). \end{aligned} \quad (15)$$

Again, we define a crossing time  $t_c^{(2)}$  for the MSD as the ratio between the absolute values of the coefficients of the  $t^3$  and  $t^4$  scalings:

$$t_c^{(2)} \simeq \frac{4D}{|2D(\mu + 3\lambda_d + \lambda_s) - v^2|}. \quad (16)$$

This approximation works for  $v^2 < 2D(\mu + 3\lambda_d + \lambda_s)$ , as otherwise the fourth order coefficient has the same sign of the third order one, and is less decisive in the change of scaling than the higher orders in time. If we change the population rates we observe that the growth or decay in the number of cells does not influence qualitatively the scalings we just described for both the MD and MSD.

Finally, we study directly the full intermediate scattering function  $\mathcal{F}(k, t)$ , as it carries more information than the MSD and MD. In Figure 5 (a), that is in the case of equal velocities, we can see that the real part of  $\mathcal{F}(k, t)$ , that generates the MSD among all other even moments, decays rapidly for small length scales (i.e. large  $k$ ) while it has three distinct regimes for large length scales. At first the function decays, then at time  $t_c^{(2)}$  it plateaus for a time that grows larger as  $k$  gets smaller, and finally decays completely. The plateau, starting after the

transition of the cell to its moving stage at time  $t_c^{(2)}$ , is generated by the active cells going back to the settled stage and not moving anymore, while the final decay represents the long time diffusive behavior that we have already seen in the MSD. In Figure 5 (b) we see how unequal velocities change the intermediate scattering function by introducing an oscillating behavior at long times. This is a signature of ballistic motion and of a nonvanishing imaginary part of  $\mathcal{F}(k, t)$ , that generates the odd moments like the MD.

## 4 Interacting cells

### 4.1 Attraction to settled regions

We want now to model an attractive force that pushes moving cells towards the regions where the density of settled cells is larger. This force is meant to represent how bacteria tend to assemble in resource-rich regions to reproduce or how they accumulate in order to form biofilms [34, 35]. We use the following mean-field potential

$$U[\rho_0] = -\kappa\rho_0, \quad (17)$$

where  $\kappa$  is a positive constant, leading to the following system of equations:

$$\begin{aligned} \partial_t \rho_+ &= -v_+ \partial_x \rho_+ - \kappa \partial_x (\partial_x (\rho_0) \rho_+) + D \partial_x^2 \rho_+ \\ &\quad - (\lambda_s + \lambda_e + \mu) \rho_+ + \lambda_e \rho_- + \lambda_d \rho_0 \\ \partial_t \rho_0 &= -\lambda_d \rho_0 + \lambda_s (\rho_+ + \rho_-) \\ \partial_t \rho_- &= v_- \partial_x \rho_- - \kappa \partial_x (\partial_x (\rho_0) \rho_-) + D \partial_x^2 \rho_- \\ &\quad - (\lambda_s + \lambda_e + \mu) \rho_- + \lambda_e \rho_+ + \lambda_d \rho_0. \end{aligned} \quad (18)$$

The interaction terms  $\kappa \partial_x (\partial_x (\rho_0) \rho_{\pm})$  make Eqs. (18) nonlinear, such that they are not analytically solvable. Instead we perform a linear stability analysis by taking the homogeneous stationary solution to the linear system  $\hat{\rho}$ , adding to it a small perturbation  $\delta\rho(x, t)$  and neglecting the nonlinear terms in the perturbation  $(\delta\rho(x, t))^2$ . We then arrive at the following linearized system of equations for the perturbation

$$\begin{aligned} \partial_t \delta\rho_+ &= -v_+ \partial_x \delta\rho_+ - \kappa \partial_x^2 (\delta\rho_0) \hat{\rho} + D \partial_x^2 \delta\rho_+ \\ &\quad - (\lambda_s + \lambda_e + \mu) \delta\rho_+ + \lambda_e \delta\rho_- + \lambda_d \delta\rho_0 \\ \partial_t \delta\rho_0 &= -\lambda_d \delta\rho_0 + \lambda_s (\delta\rho_+ + \delta\rho_-) \\ \partial_t \delta\rho_- &= v_- \partial_x \delta\rho_- - \kappa \partial_x^2 (\delta\rho_0) \hat{\rho} + D \partial_x^2 \delta\rho_- \\ &\quad - (\lambda_s + \lambda_e + \mu) \delta\rho_- + \lambda_e \delta\rho_+ + \lambda_d \delta\rho_0. \end{aligned} \quad (19)$$

We perform perturbations to the stationary solution  $\hat{\rho}$  of a homogeneous system (without interaction), which

was computed in Eq. (7) (see also Fig. 3). Now, we apply both a Fourier transform in space and a Laplace transform in time to Eq. (19) and solve the resulting characteristic equation of the system. We obtain three different solutions for the eigenvalues of the system  $s_i(k)$ , of which only one,  $s_1(k)$ , has a positive real part. In the following we focus on  $s_1(k)$ , since its positive real part introduces instabilities in the system.

First of all, for  $k \rightarrow 0$ , the value of  $s_1(k)$  is one of the eigenvalues of the system matrix where the initial densities are constant, and more specifically the one that can be positive:

$$s_1(0) = \mathcal{E}_3 \simeq \frac{\lambda_d(\lambda_s - \mu)}{\mu + \lambda_d + \lambda_s}. \quad (20)$$

This means that one of the conditions for the system to be stable is that the number of cells does not grow exponentially, which is expected.

The second limit we consider is  $k \rightarrow \infty$ . We have that

$$\lim_{k \rightarrow \infty} s_1(k) \rightarrow \frac{2\kappa\hat{\rho}\lambda_s}{D} - \lambda_d. \quad (21)$$

This second condition states that the diffusion constant contrasts directly the instabilities generated by a large sticking rate and the attractive constant  $\kappa$ , as it disperses too large clusters of active cells, while a large doubling rate helps the stability by reducing the size of groups of settled cells. Knowing the limits of  $s_1(k)$  in 0 and  $\infty$ , which are both real, we are sure that the system will be unstable if either of them is larger than zero, giving us two stability conditions for the system:

$$\begin{aligned} \mu &\geq \lambda_s, \\ \lambda_d &\geq \frac{2\kappa\hat{\rho}\lambda_s}{D}. \end{aligned} \quad (22)$$

For  $D = 0$ ,  $s_1(k)$  grows asymptotically like  $k$ , making the system always unstable. We remark that the first stability condition is more relevant for long range perturbations, while the second one is important for small scales. In Figure 6 we show the behavior of the eigenvalue  $\text{Re}(s_1(k))$  for different values of  $D$ . Notice that for the set of parameters considered, if  $D = 2v_+^2/\lambda_e$  the stability conditions are only narrowly fulfilled, but the real part of  $s_1$  stays negative for all the values of  $k$ . Lastly, when the cell active velocities are not isotropic, the imaginary part of  $s_1$  can be non-zero, meaning that there can be stable periodicity in the system. While the real part of the other two solutions  $s_2$  and  $s_3$  is always negative, their imaginary part is non-zero for large values of  $k$ . More specifically, for large  $k$  and finite  $D$  their imaginary part is proportional to  $k$ , while the real part goes with  $-Dk^2$ . A finite imaginary part indicates oscillations in the system, although the negative real

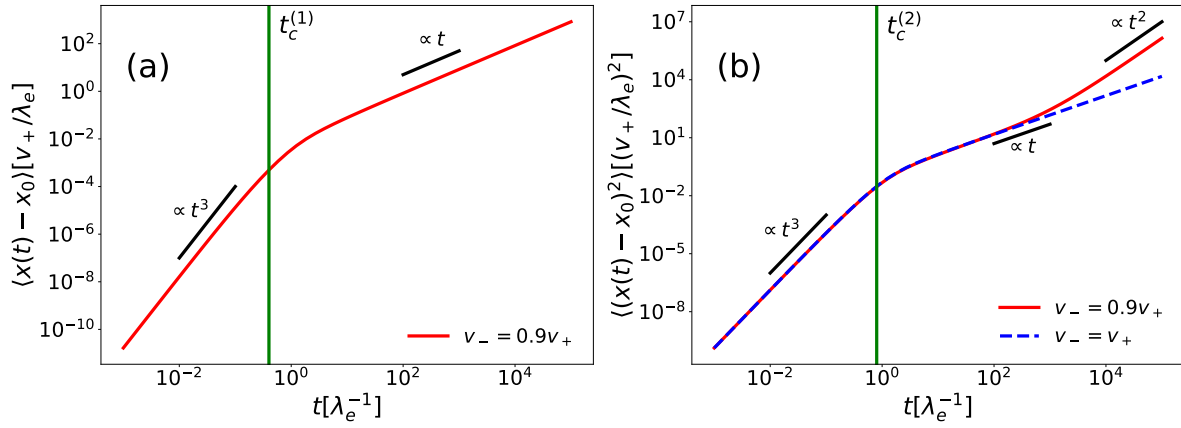


**Fig. 4** (a) Mean displacement (MD), (b) mean-square-displacement (MSD) and respective crossing times  $t_c^{(1)}$ ,  $t_c^{(2)}$  for the initial conditions  $\rho(x, 0) = (0, \delta(x), 0)$ , all rates equal to  $\lambda_e$  and  $D = 0.2v_+^2/\lambda_e$ . In (b) the solid line shows unequal swim velocities ( $v_- = 0.9v_+$ ) and the dashed line equal swim speeds ( $v_- = v_+$ ).

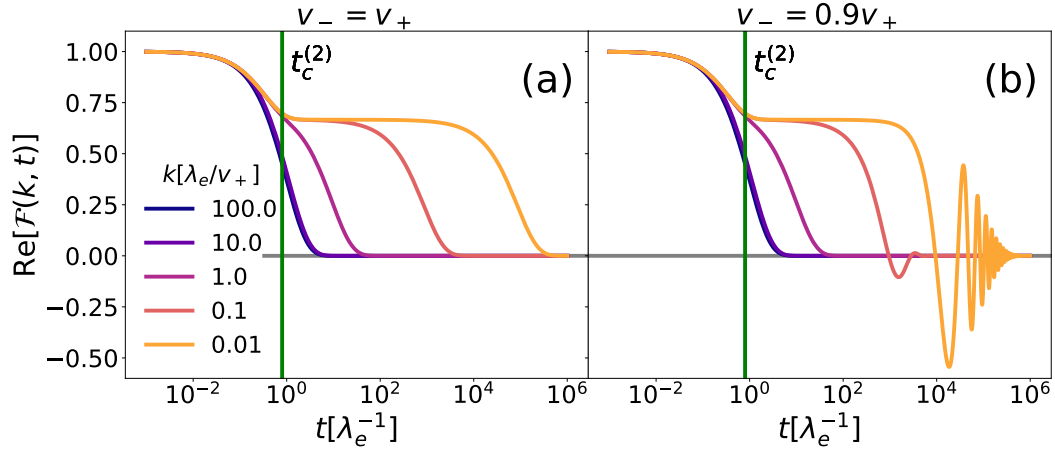


**Fig. 5** Real part of the intermediate scattering function  $\mathcal{F}(k, t)$  for (a) equal swimming speeds and (b) unequal swimming speeds ( $v_- = 0.9v_+$ ) for the initial conditions  $\rho(x, 0) = (0, \delta(x), 0)$ , all rates equal to  $\lambda_e$  and  $D = 0.2v_+^2/\lambda_e$ . The green lines represent the MSD crossing time  $t_c^{(2)}$ .

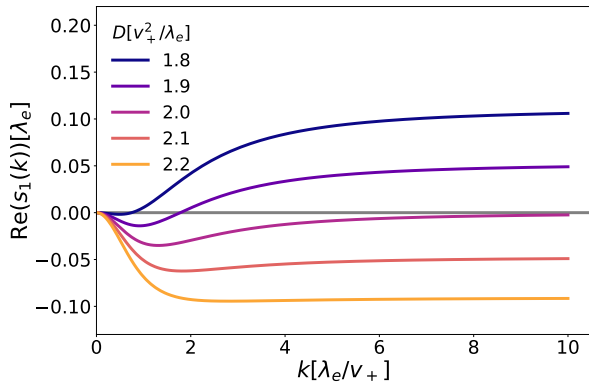


**Fig. 6** Eigenvalue  $s_1(k)$  as a function of wavenumber  $k$  for different values of  $D$ , where all rates are equal to  $\lambda_e$ ,  $v_- = v_+$  and  $\kappa = \lambda_e^{-1}$ .

part means that these oscillations are only transient. Signatures of these oscillations can also be seen in our numerical solutions (see the next Section).

#### 4.2 Repulsion among settled cells

We now include a self-repulsive potential for the cells that do not move, given by

$$V[\rho_0] = \kappa_0 \rho_0, \quad (23)$$

where  $\kappa_0$  is a positive constant, leading to

$$\begin{aligned}\partial_t \rho_+ &= -v_+ \partial_x \rho_+ - \kappa \partial_x (\partial_x (\rho_0) \rho_+) + D \partial_x^2 \rho_+ \\ &\quad - (\lambda_s + \lambda_e + \mu) \rho_+ + \lambda_e \rho_- + \lambda_d \rho_0 \\ \partial_t \rho_0 &= \kappa_0 \partial_x (\partial_x (\rho_0) \rho_0) - \lambda_d \rho_0 + \lambda_s (\rho_+ + \rho_-) \\ \partial_t \rho_- &= v_- \partial_x \rho_- - \kappa \partial_x (\partial_x (\rho_0) \rho_-) + D \partial_x^2 \rho_- \\ &\quad - (\lambda_s + \lambda_e + \mu) \rho_- + \lambda_e \rho_+ + \lambda_d \rho_0.\end{aligned}\quad (24)$$

This repulsion models the need for settled bacteria to not overcrowd any particular region and deplete its resources while reproducing. What is particularly interesting about having an attractive potential  $U[\rho_0]$  and repulsive potential  $V[\rho_0]$  is that the interplay of these two opposing effects can lead to structures forming in the system, as we will show now. The complexity of the full nonlinear equations in this case does not allow for analytical approaches. Thus in order to study the nonlinear system Eqs.(24), we implemented a numerical solver, using an explicit fourth order Runge-Kutta algorithm [36] for the time integration and a finite difference scheme in space. We use a finite box of length  $L$  with periodic boundary conditions. Our time step is fixed to  $\Delta t = 10^{-4} \lambda_e^{-1}$ , and we simulated  $\sim 10^6$  steps to ensure that the system settles into a steady state. Our simulations are initialized using the steady state solutions of the linear system (Eqs. (7)), to which we add small fluctuations (Gaussian noise). Furthermore, we set  $\mu = \lambda_s$  to avoid the exponential growth or collapse of the system.

We find that our system develops wave-like structures, which are static for  $v_+ = v_-$  and become traveling waves when we have  $v_+ \neq v_-$  (see Figure 7). What is particularly surprising here is that in this final stationary state all three species of cell move on average in the same direction at the same speed, independently of their intrinsic active velocity. Clearly, the wave-like behavior is dominated by the speeds of right  $v_+$  and left  $v_-$  moving cells. Hence, we quantify their occurrence using two non-dimensional parameters, the maximum speed  $v_m$  and the reduced difference speed  $v_r$  defined by

$$v_m \equiv \frac{\max(v_+, v_-)}{\sqrt{D\lambda_e}} \quad v_r \equiv \frac{v_+ - v_-}{v_+ + v_-}. \quad (25)$$

The resulting non-equilibrium state diagram is shown in Figure 8. We find a clear transition from a stable system (in blue), where all species are constant in space, to the creation of wavelike structures (in red to yellow). The gradient visualizes the change in stationary speed of the waves  $v_s$ , defined as the speed of the waves in the stationary state divided by  $\sqrt{D\lambda_e}$ , and is hence non-dimensional. This is almost vanishing near the transition, and grows the further away we move from it. The

formation of such waves is typical of systems with large difference between  $v_+$  and  $v_-$  or rather small absolute speeds. We fitted the separation line to a second order polynomial  $v_r^f(v_m)$ , obtaining:

$$v_r^f = -0.26 \pm 0.04 - (0.13 \pm 0.02)v_m + (0.077 \pm 0.003)v_m^2. \quad (26)$$

This particular fit was calculated considering as parameters  $\lambda_s = \lambda_d = \mu = 0.1\lambda_e$ ,  $\kappa = 0.2\lambda_e^{-1}$ ,  $\kappa_0 = 0.05\lambda_e^{-1}$  and  $D = 0.001L^2\lambda_e$ .

## 5 Conclusions and outlook

In this work we proposed and studied a 1D 3-state model motivated by the cell cycle progression of the bacterium *Caulobacter crescentus*, including both its run and tumble motion and its reproductive behavior. We first analyzed the free cell space-independent case and calculate the parameter regimes for which the number of cells grows or declines. Adding the spatial dependence we subsequently determined dynamical quantities of the system, such as mean displacement, mean squared displacement and intermediate scattering function. We found a surprising super-ballistic behavior of the MSD at short times with a  $t^3$  scaling, which stems from interplay of cells doubling and cells starting to swim. Subsequently, we included attractive and repulsive interactions between cells into our model, representing their tendency to swim towards regions in which cells are settled and their mutual exclusion. We determined the stability conditions and, using numerical methods, we studied the fully nonlinear system in which we identify traveling waves of cells. Their occurrence was quantified in a non-equilibrium state diagram.

Our model lends itself to still further extensions in several ways. E.g., one could account for complex nutrient landscapes and for a more detailed description of the cell cycle, which is well-studied from various aspects [27]; another possible system for application are *Chlamydomonas reinhardtii* cells [28]. The cell cycle can be included in cell-resolved simulations such as performed recently in [37, 38]. Another direction could be a two-dimensional field description that includes the nematic ordering of cells such as in [39].

## Appendix

We show here the calculation that justifies Eq.(12) in one dimension in the case where the initial conditions for the cell density are  $\rho(x, t=0) = N(0)\delta(x)$ . First, we

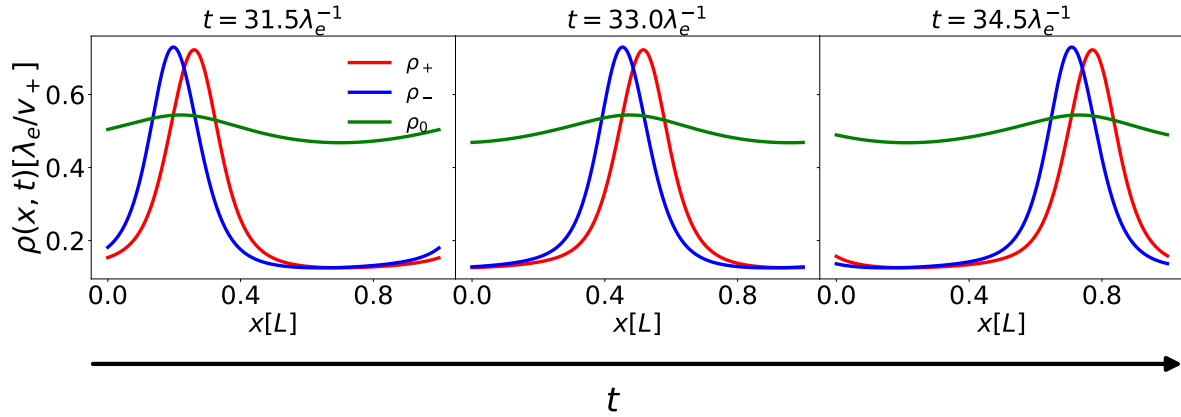


**Fig. 7** Density of left  $\rho_-$ , right  $\rho_+$  and sedentary  $\rho_0$  cells as functions of space at different times (increasing from (a) to (c)). We set here  $\lambda_s = \lambda_d = \mu = .1\lambda_e$ ,  $\kappa = .2\lambda_e^{-1}$ ,  $\kappa_0 = .05\lambda_e^{-1}$ ,  $v_+ = 2v_- = .1L\lambda_e$  and  $D = 0.001L^2\lambda_e$ .

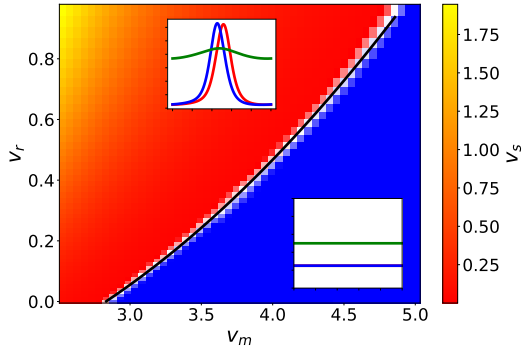


**Fig. 8** State diagram of the system as a function of  $v_r$  and  $v_m$ . As parameters we chose  $\lambda_s = \lambda_d = \mu = 0.1\lambda_e$ ,  $\kappa = 0.2\lambda_e^{-1}$ ,  $\kappa_0 = 0.05\lambda_e^{-1}$  and  $D = 0.001L^2\lambda_e$ . In blue we see the parameters for which the system is stably constant, while in red to yellow we see the parameters for which the system generates traveling wave structures. Examples of both long-time behaviors are shown in their respective area. The gradient shows the stationary velocity of the waves  $v_s$ , while in black we have the second order polynomial that fits the transition curve  $v_r^f$ .

write the definition for the moments  $\langle (x(t) - x_0)^n \rangle = \langle x^n(t) \rangle$ :

$$\langle x^n(t) \rangle = \int_{-\infty}^{\infty} dx x^n P(x, t), \quad (27)$$

where  $P(x, t)$  is the probability density of the position. We then apply a Fourier transform and its inverse in the integral

$$\langle x^n(t) \rangle = \frac{1}{2\pi} \int_{-\infty}^{\infty} dx \int_{-\infty}^{\infty} dk e^{ikx} \left( i^n \frac{\partial^n \tilde{P}(k, t)}{\partial k^n} \right), \quad (28)$$

where  $\tilde{P}(k, t)$  is the Fourier Transform of  $P(x, t)$ . Finally, we exchange the order of integration to get

$$\begin{aligned} \langle x^n(t) \rangle &= \frac{1}{2\pi} \int_{-\infty}^{\infty} dk 2\pi \delta(k) \left( i^n \frac{\partial^n \tilde{P}(k, t)}{\partial k^n} \right) \\ &= i^n \frac{\partial^n \tilde{P}(k, t)}{\partial k^n} \Big|_{k=0}. \end{aligned} \quad (29)$$

Knowing that  $\tilde{P}(k, t) = \tilde{\rho}(k, t)/N(t)$  and that for the initial conditions that we chose  $\tilde{\rho}(-k, 0) = N(0)$ , we have that

$$\mathcal{F}(k, t) \equiv \frac{\tilde{\rho}(k, t)\tilde{\rho}(-k, 0)}{N(0)} = \tilde{\rho}(k, t) = \tilde{P}(k, t)N(t), \quad (30)$$

and hence

$$\langle x^n(t) \rangle = i^n \frac{\partial^n \tilde{P}(k, t)}{\partial k^n} \Big|_{k=0} = \frac{i^n}{N(t)} \frac{\partial^n \mathcal{F}(k, t)}{\partial k^n} \Big|_{k=0}. \quad (31)$$

## Acknowledgements

DB is supported by the EU MSCA-ITN ActiveMatter, (proposal No. 812780). RB is grateful to HL for the invitation to a stay at the Heinrich-Heine-University in Düsseldorf where this work was performed. HL was supported by the DFG project LO 418/25-1 of the SPP 2265.

## Author contribution statement

HL and RB directed the project. DB performed analytic calculations and numerical simulations. All authors discussed the results and wrote the manuscript.

## References

1. Berg H C (ed) 2004 *E. coli in Motion* Biological and Medical Physics, Biomedical Engineering (New York, NY: Springer) ISBN 978-0-387-00888-2 978-0-387-21638-6
2. Polin M, Tuval I, Drescher K, Gollub J P and Goldstein R E 2009 *Science* **325** 487–490
3. Elgeti J, Winkler R G and Gompper G 2015 *Reports on Progress in Physics* **78** 056601
4. Angelani L 2017 *Journal of Physics A: Mathematical and Theoretical* **50** 325601
5. Detcheverry F 2017 *Physical Review E* **96** 012415
6. Berg H C 2018 *Random Walks in Biology: New and Expanded Edition* (Princeton University Press) ISBN 978-1-4008-2002-3
7. Bertrand T, Illien P, Bénichou O and Voituriez R 2018 *New Journal of Physics* **20** 113045
8. Fier G, Hansmann D and C Buceta R 2018 *Soft Matter* **14** 3945–3954
9. Angelani L and Garra R 2019 *Physical Review E* **100** 052147
10. Dhar A, Kundu A, Majumdar S N, Sabhapandit S and Schehr G 2019 *Physical Review E* **99** 032132
11. Dandekar R, Chakraborti S and Rajesh R 2020 *Physical Review E* **102** 062111
12. Garcia-Millan R and Pruessner G 2021 *Journal of Statistical Mechanics: Theory and Experiment* **2021** 063203
13. Singh P, Sabhapandit S and Kundu A 2020 *Journal of Statistical Mechanics: Theory and Experiment* **2020** 083207
14. Zhang Z and Pruessner G 2022 *Journal of Physics A: Mathematical and Theoretical* **55** 045204
15. Singh P and Kundu A 2021 *Physical Review E* **103** 042119
16. Le Doussal P, Majumdar S N and Schehr G 2021 *Physical Review E* **104** 044103
17. Barriuso Gutiérrez C M, Vanhille-Campos C, Alarcón F, Pagonabarraga I, Brito R and Valeriani C 2021 *Soft Matter* **17** 10479–10491
18. Monthus C 2021 *Journal of Statistical Mechanics: Theory and Experiment* **2021** 083212
19. Mori F, Gradenigo G and Majumdar S N 2021 *Journal of Statistical Mechanics: Theory and Experiment* **2021** 103208
20. Frydel D 2021 *Journal of Statistical Mechanics: Theory and Experiment* **2021** 083220
21. Maes C, Meerts K and Struyve W 2022 *Physica A: Statistical Mechanics and its Applications* 127323
22. Frydel D 2022 *Physical Review E* **105** 034113
23. Basu U, Majumdar S N, Rosso A, Sabhapandit S and Schehr G 2020 *Journal of Physics A: Mathematical and Theoretical* **53** 09LT01
24. Grange P and Yao X 2021 *Journal of Physics A: Mathematical and Theoretical* **54** 325007
25. Frydel D 2022 *Physics of Fluids* **34** 027111
26. Shebelut C W, Guberman J M, van Teeffelen S, Yakhnina A A and Gitai Z 2010 *Proceedings of the National Academy of Sciences* **107** 14194–14198
27. Biondi E (ed) 2022 *Cell Cycle Regulation and Development in Alphaproteobacteria* (Cham: Springer International Publishing) ISBN 978-3-030-90620-7 978-3-030-90621-4
28. Harris E, Stern D and Witman G 2009 *The Chlamydomonas Sourcebook* **1**
29. Li G and Tang J X 2006 *Biophysical Journal* **91** 2726–2734
30. Lin Y, Crosson S and Scherer N F 2010 *Molecular Systems Biology* **6** 445
31. Liu B, Gulino M, Morse M, Tang J X, Powers T R and Breuer K S 2014 *Proceedings of the National Academy of Sciences* **111** 11252–11256
32. Lele P P, Roland T, Shrivastava A, Chen Y and Berg H C 2016 *Nature Physics* **12** 175–178
33. Kurzthaler C, Leitmann S and Franosch T 2016 *Scientific Reports* **6** 36702
34. Hall-Stoodley L, Costerton J W and Stoodley P 2004 *Nature Reviews Microbiology* **2** 95–108
35. Mazza M G 2016 *Journal of Physics D: Applied Physics* **49** 203001
36. Press W H, Teukolsky S A, Vetterling W T and Flannery B P 2007 *Numerical Recipes 3rd Edition: The Art of Scientific Computing* (Cambridge University Press) ISBN 978-0-521-88068-8
37. You Z, Pearce D J, Sengupta A and Giomi L 2018 *Physical Review X* **8** 031065
38. Schwarzendahl F J and Beller D A 2022 arXiv:2205.05185 [cond-mat, q-bio]
39. Dell’Arciprete D, Blow M L, Brown A T, Farrell F D C, Lintuvuori J S, McVey A F, Marenduzzo D and Poon W C K 2018 *Nature Communications* **9** 4190